




Electrical properties of Lithium silicate-based glasses and their Glass-ceramics

Esmat M. A. Hamzawy^{1,*} , Gehan T. El-Bassyouni², Moenis A. Azooz¹, and Gamal M. Turkey³

¹ Glass Research Department, National Research Centre (NRC), 33-El Buhouth St., Dokki, Cairo 12622, Egypt

² Refractories, Ceramics and Building Materials Department, National Research Centre (NRC), 33-El Buhouth St., Dokki, Cairo 12622, Egypt

³ Microwave Physics Department, National Research Centre (NRC), 33-El Buhouth St., Dokki, Cairo 12622, Egypt

Received: 2 September 2023

Accepted: 8 January 2024

Published online:
29 January 2024

© The Author(s), 2024

ABSTRACT

Crystallization of lithium di- and meta-silicates were developed in the SiO_2 - Li_2O - TiO_2 glass system. Inclusion of TiO_2 relatively reduced the crystallization temperature. Through the sintering process at $650\text{ }^\circ\text{C}/2\text{ h}$, lithium disilicate was devolved in the TiO_2 -free sample, whereas the incorporation of TiO_2 catalyzed the appearance of lithium metasilicate phases. The microstructure of lithium disilicate glass-ceramics was studied using differential thermal analysis (DTA), powder X-ray diffraction (PXRD), and scanning electron microscopy (SEM). At $650\text{ }^\circ\text{C}/2\text{ h}$, the microstructure consists of spherulitic growths with reasonably sorted nanosize particles in a glassy groundmass. The electrical characteristics of lithium silicate glasses and glass-ceramics having variable concentrations of TiO_2 were tested in order to explore their electronic hopping process. To clarify the effects of composition and sintering on the electrical and dielectric behavior of glasses based on lithium silicate, a Broadband Dielectric Spectroscopy (BDS) was employed. While the matching-sintered glass-ceramic exhibits like an insulator with interfacial polarization that significantly lowers the density number of free ions, bulk glass nevertheless demonstrate high conductivity. Lithium oxide considerably increases the conductivity of the composite instead of titanium oxide.

1 Introduction

Glass-ceramic is a polycrystalline material designed by adjusting crystal phases confined by the glass's crystallization and development [1]. As nucleating agents, transition metal oxides and sulfides, such as zirconium dioxides (ZrO_2) and titanium dioxides (TiO_2), are typically employed [2]. There are four, five, and six coordination modes of Ti^{4+} in the glass network, which exist

in the geometric form of tetrahedra, square pyramids, and octahedra, respectively. $[\text{TiO}_4]$ is a network former to form a glass network framework, $[\text{TiO}_6]$ is a network modifier, and $[\text{TiO}_5]$ has a square pyramidal structure with four Ti-O single bonds and one Ti=O double bond [3, 4]. The declared system is a fundamental component of glass and glass ceramics [5]. It is noteworthy that transparent glasses can initially be found in large quantities, in a fine region close to the

Address correspondence to E-mail: ehamzawy9@gmail.com

lithium disilicate (LS_2), which is classified as a glass-ceramic, in the category of particle-filled glass materials [6, 7]. In contrast to compositions richer in Li_2O , which rapidly crystallize to produce the binary system of lithium silicate (Li_2SiO_3), compositions richer in silica gloomily melted [8]. The interaction of titanium and silicon dioxides in the formation of ceramics, glass ceramics, and glasses must be understood in terms of the SiO_2 - TiO_2 system [9]. The sizable region of liquid immiscibility and lack of binary compounds are two characteristics that set the SiO_2 - TiO_2 system apart from other structural systems. With an increase in SiO_2 content, crystallization progresses more slowly. No equilibrium data have been reported for the ternary system Li_2O - TiO_2 - SiO_2 . The order of the produced phases was proven to be unaffected by the employment of alkali and divalent metal oxides as technological additives; however, they did speed up the liquid phase separation and glass crystallization via the TiO_2 [10]. The development of different crystalline phases depends on the original composition, increasing the SiO_2 concentration while simultaneously reducing the Li_2O concentration, as well as the thermal treatment conditions [11]. In the lithium disilicate glass-ceramic system, the SiO_2 : Li_2O ratio is an important success factor in the creation of the primary crystal phase. Crystallization is achieved through repeated thermal processing, leading to the production of glass-ceramic. Lithium titanate silicate ($\text{Li}_2\text{TiSiO}_5$) and lithium silicate (Li_2SiO_3) are likely the two major crystal phases that separate. The degree of crystallization was reduced as the SiO_2 content was increased [12]. It was anticipated by Monmatrapoj et al., 2013 that a change in the microstructure of the lithium disilicate crystals was caused by the Si:Li ratio in glass compositions rising [13]. Titanium dioxide TiO_2 is a well-known and well-probed material because of its biocompatibility, chemical, physical, optical, and electrical properties. Titanium dioxide is an n-type semiconductor having a wide bandgap ranging from 3 to 3.2 eV. It has a high refractive index which is $n = 2.614$. Consequently, by adding titania to glass, the optical bandgap is altered, causing the electrical resonance in the ultraviolet spectral range to shift to a longer wavelength [14].

This task of the current study suggests the glass co-derived from the Li_2O - TiO_2 - SiO_2 system to investigate how the glass composition affects the crystal characteristics and forms. Glasses were made by melting in a platinum crucible, frequently in a Globar oven but sporadically in a gas-fired pot furnace

for some of the high-melting compositions. All glass ceramics will be identified by X-ray diffraction, DTA, and SEM. Using electron microscopy and quenching data, in the binary system SiO_2 - TiO_2 will extend over a substantial portion of the ternary system. BDS was performed to investigate the effect of composition, and sintered glasses at 650 °C/2 h on the dielectric behavior of ternary system. Broad exploration by solid-state reactions in the prepared system exposed the existence of the ternary compound Li_2O - TiO_2 - SiO_2 .

The use of the glass-ceramic solid electrolytes leads to the development of a bulk-type all solid-state lithium secondary battery with excellent cycling performance. Even though, the lithium silicate glass is one of the promising candidate materials as solid electrolyte in a secondary battery but it has a low ionic conductivity. To enhance the ionic conductivity of lithium silicate glass, we synthesize a couple of the high concentration Li ions of lithium silicate glass.

A non-invasive method called "Broadband Dielectric Spectroscopy" (BDS) can be used to determine where and how much the system's primary polar components-electrical dipoles within the molecules are influencing the system as a whole. It can probe all the dynamics at the molecular and sub-molecular scales in the material and the mechanisms of charge transport in a disordered compressed material over a broad frequency ranges within 12 decades [15, 16]. The different complex functions like dielectric permittivity $\epsilon^*(\nu)$, electric modulus $M^*(\nu)$, and ac conductivity $\sigma^*(\nu)$ are connected by a direct relationship. Despite being derived from that range of temperatures and frequencies, these complex parameters may emphasize other features. The fluctuation is often represented in terms of ϵ^* in condensed matter physics, while the electric conduction behavior is typically characterized in terms of σ^* , Z^* , or M^* . In advanced materials, complex conductivity $\sigma^*(x)$ or complex electric modulus $M^*(x)$ are typically alternative demonstrations of the dielectric properties. They support many aspects of polarization and charge transport in a material. The composition of the considered glasses was varied while conducting the current investigation, and when the considered glasses evolved into glass ceramics, the dielectric and electrical properties were examined utilizing BDS. The three main complex functions, that is, (ϵ^*), (σ^*), and (M^*) are equivalent, although they often are used to highlight various elements of the molecular dynamic relaxation and charge carriers' transit

underlying processes. The three parameters are inter-related with each other according to Eq. (1):

$$M^* = \frac{1}{\epsilon^*} = \frac{i\omega\epsilon_0}{\sigma^*}. \quad (1)$$

The relationship between these functions and others can be found in some details elsewhere [17–19].

Due to the appropriate dielectric properties of the advanced glasses and glass ceramics, the present work introduces a new application for electric insulators and semiconductor purposes. There is now huge attention in this research field owing to their expanded use in fields comprising electronic, optical, and storage devices [20, 21]. But, there are challenges concerning changes in their electrical properties and thermal stability. For example, density and permittivity can be easily altered as a result of processing techniques, including annealing and sintering, since the sintering process is employed to create the various crystalline phases in quenched glasses [22]. The nature of atomic bonds, bond length, polarizability of the constituents, and crystalline phases can all be factors in the change in characteristics (dielectric constant and dielectric loss). The dielectric constant usually called permittivity is the real part of the complex dielectric function and defined as a measure of the material's ability to store electrical energy. However, the dielectric loss, the imaginary part of the complex dielectric function is a measure of the energy absorbed in the material. It was standing that in case of forming new non-bridging oxygens in silicate glass, directly the number of hopping sites can be enhanced. This makes the transport of ions easier.

2 Experimental and materials

Three glasses compositions were prepared within Li_2O – TiO_2 – SiO_2 system with fixed ratio of Li_2O (20%) and different TiO_2 and SiO_2 ratios (Fig. 1 and Table 1). The starting materials were lithium carbonate (Li_2CO_3 , Cl: 0.01%, SO4: 0.01%, Fe: 0.002, Pb: 0.001, BDH—England), titanium dioxide (TiO_2 , 98%, Fe: 0.05%, BDH—England), and silica sand (local Silica' sand SiO_2 :99.5). The well-mixed powder batches were melted in a platinum crucible at 1250 °C for two hours. Part of poured melted sample was shaped as rods then transferred to an annealing furnace (pre-heated at 450 °C) and the residual one was quenched with water to form glass frits. The frits of glass were crushed using a ball mill

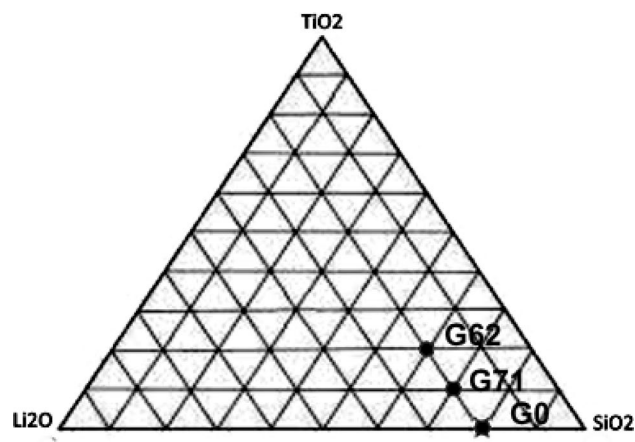


Fig. 1 Glass compositions through the Li_2O – TiO_2 – SiO_2 system

Table 1 Compositions of the glass batches

Oxides	Glass compositions in wt%		
	G0	G71	G62
SiO_2	80	70	60
TiO_2	–	10	20
Li_2O	20	20	20
Melting Temp. about	1250	1250	1250
Product	Glass	Glass	Glass

to develop powder of grain size < 0.083 mm. The glass powder was shaped in the form of disk after being subjected to sintering at 650 °C/ 2 h. Afterward, the rods after annealing were used in electrical properties.

2.1 Characterization

The thermal behavior of the glass samples was tested using differential thermal analysis (DTA-STDQ 600 TA-USA). The glass powder (~ 20 mg) was used against inert alumina as reference at a 10 °C/min heating rate in a nitrogen environment and samples holder was open.

A Broadband Dielectric Spectroscopy, BDS, is performed to investigate the effect of composition and sintered glasses at 650 °C/2 h on the dielectric behavior of ternary system of SiO_2 – Li_2O – TiO_2 glasses. BDS utilizes Novocontrol Technologies, GmbH & Co. KG, high-resolution alpha analyzer in the frequency window ranging from 0.1 Hz up to 20 MHz. The sample cell consists of two parallel plate capacitors made of 10 mm diameter stainless steel disk electrodes. To

remove any further influences from the cables and the measurement cell, the sample capacitor that was empty from the sample was utilized as a reference in this case. The adjusted sample thickness typically differs from the thickness determined using a digital micrometer. BDS was provided with a Win data software application so that it could determine the sample's electrical and dielectric properties from the output parameters. Every investigation was done at room temperature.

The crystalline phases after sintering process were carried out using powder X-ray diffraction analysis (PXRD-model BRUKER Axs, D8 ADVANCE, Germany). The X-ray diffraction spectra were examined over 2θ range from 2 to 60° using Cu-K α radiation (wavelength = 1.54056 Å, current 40 mA and applied voltage 40 kV) through a scanning speed of 2° in 20 min^{-1} .

The microcrystalline structure was studied by means of scanning electron microscopy (SEM, Philips-XL30, the Netherlands). The SEM micrographs of the crystalline samples were scanned on the freshly fractured surfaces after chemical etching (using 1% HF + 1% HNO₃ for 30 s) and then rinsed with distilled water before being scanned.

3 Results and discussion

3.1 Characterization

The melting temperatures of the prepared batches were $\sim 1250^\circ\text{C}$ (Table 1). The thermal behavior of the glass samples exhibited a clear exothermic effect, whereas the endothermic effect was not clear (Fig. 2). The DTA curves show the absence of the endothermic and clear exothermic effect. However, the function of TiO₂ insertion in simulating the ratio of SiO₂ in altering the location of the exothermic peak temperature as denoted in Fig. 2. In general, the incorporation of TiO₂ led to lowering the exothermic peak from 683°C in G0 to 626°C in G62, such notification clears the role of TiO₂ in catalyzing the crystallization to lower temperature. The sintering process of the G0, G71, and G62 glasses at $650^\circ\text{C}/2 \text{ h}$ revealed the crystallization of the lithium disilicate (Li₂Si₂O₅, ICDD 96-231-0436) and lithium metasilicate (Li₂SiO₃, ICDD 96-231-0663). Therefore, it seemed clearly that the incorporation of TiO₂ lead to the appearance of both lithium silicate phases (Fig. 3).

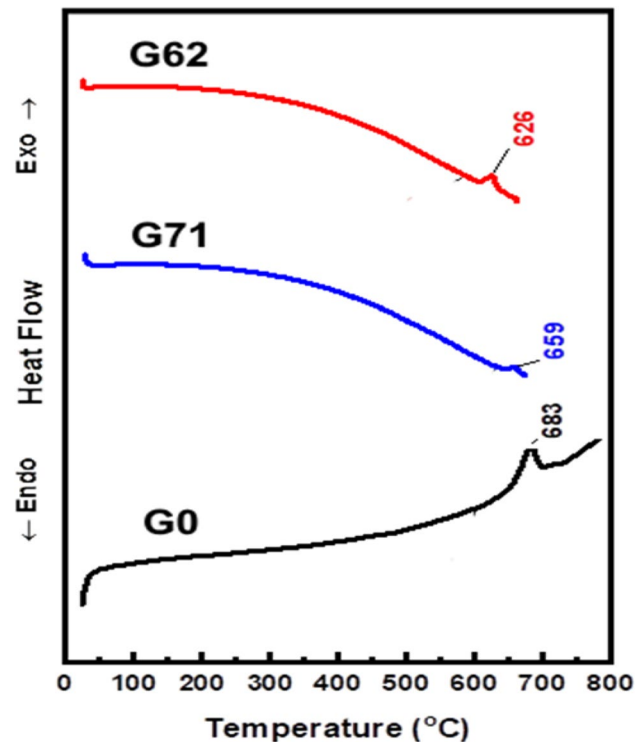


Fig. 2 DTA curves of the prepared present glasses

The scanning electron micrographs (SEM) of sintered glasses at $650^\circ\text{C}/2 \text{ h}$ are presented in Fig. 4. Clear spherulitic growths were present in all G0, G71, and G62 samples. These spherulitic growths appeared as overlapping sheets in which, each sheets enclosed spread of nanosize particles of glassy groundmass. The nanoparticles were relatively well sorted (in the range of 40 and 100 nm). The role of TiO₂ in forming the sinters for the nanosize microstructure was accompanied with the presence of the Li₂O which facilitates the mobility of the SiO₂ and the formation of both lithium meta- and disilicate phases.

3.2 Dielectric spectroscopy investigations

Figure 5 shows the change in relative permittivity (ϵ') and the inset shows the dielectric loss (ϵ'') of the three considered samples against frequency (Fig. 5). At higher frequencies starting from 10 kHz, no effect of frequency on the permittivity of the samples noticed here. Also, the permittivity values of the six investigated samples (that is glasses and glass-ceramics) are collapsed in one decade. This can be explained according to the fact that the change of the externally applied electric field is followed by a delay in all taken

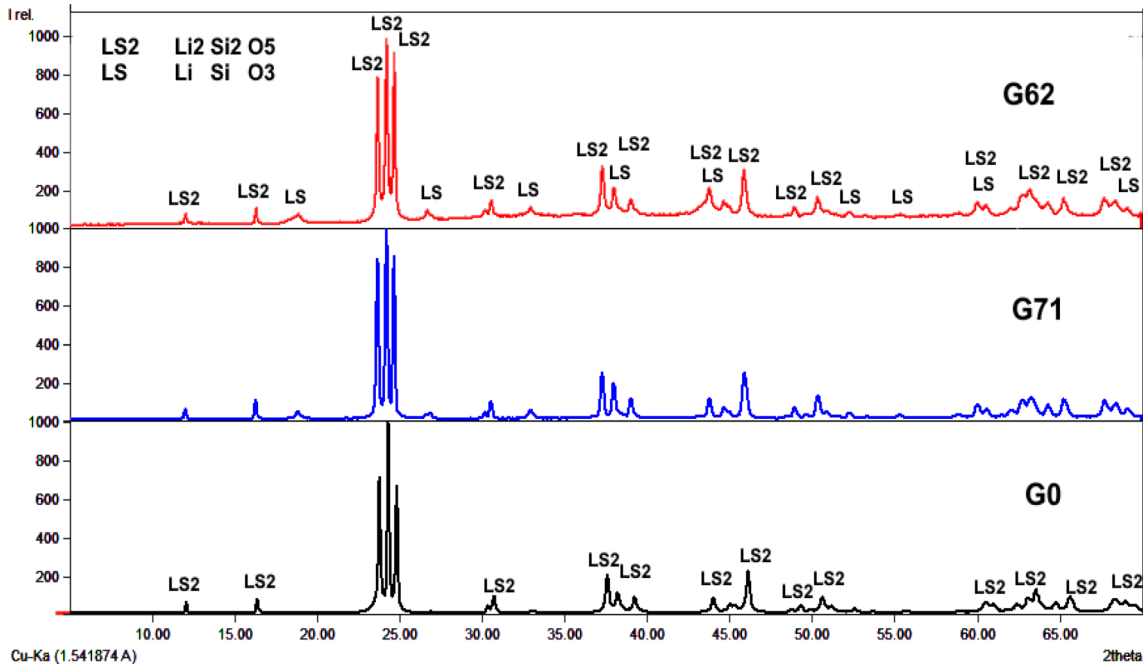


Fig. 3 X-ray diffraction patterns of G0-, G71-, and G62-sintered glasses at 650 °C/2 h

into account dynamics. Further decrease of frequency rather than 10 kHz shows abrupt and linear increase of permittivity of the glass samples. This reflects the contribution of dc conductivity of the prepared glasses originated from the free Li^+ ions. One has to conclude that, at the lower frequencies, the ions and charge accumulation have enough time, so they have responsibility to increase permittivity in the glass samples [23–25].

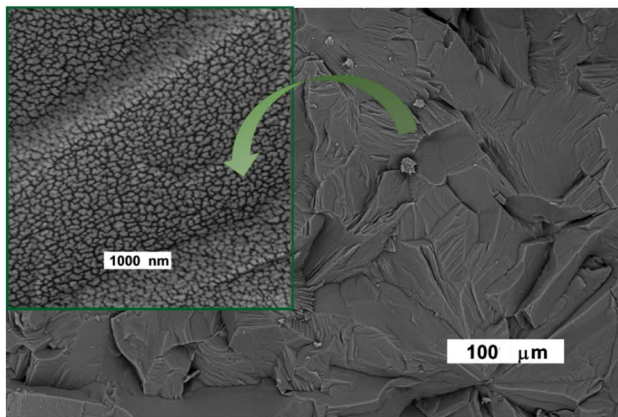
The permittivity decreases as the TiO_2 increases. The dielectric loss spectra show gradual increase of ε'' with decreasing frequency without any indication of dynamic peak behavior in case of glass samples (Fig. 5).

The sintering process of the G0, G71, and G62 glasses at 650 °C/2 h revealed a semi-crystalline structure. The incorporation of TiO_2 leads to the appearance of both lithium silicate phases and hence the heterogeneous-like structure. This explains the peak like behavior at higher frequency range that originated from the buildup of charge carriers during the transition between the crystalline and glassy phases. This leads to a remarkable reduction of permittivity and the conductivity as well in the glass ceramics. TiO_2 seems to act as a glass former which poses strong glass network and hinders the ionic motion. On the other hand, one has to think about the reduction of porosity (increase of density) upon heat treatment of

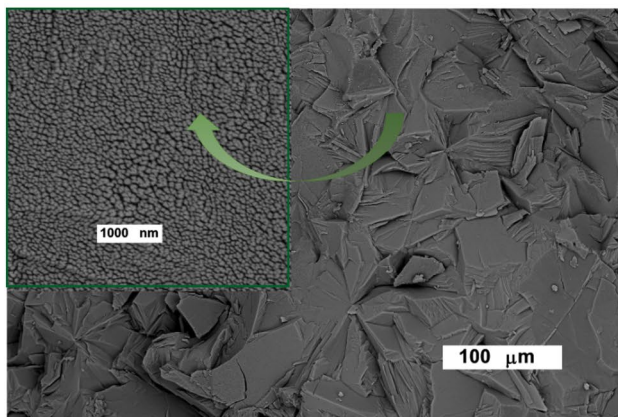
the glasses. In addition to the interfacial polarization that blocked huge number of free charge carriers, the increase of density could be responsible in reducing the dielectric constant [25–27].

Figure 6 displays clearly how ac conductivity has been affected after being subjected to sintering at 650 °C/2 h. Apart from the case of TiO_2 free sample (G0), there is a remarkable reduction of conductivity. The substitution of 10 wt% SiO_2 by TiO_2 (G71) shows the optimum reduction of conductivity that reaches four orders of magnitude lower than that of its glass sample at the lowest measured frequency point (0.1 Hz).

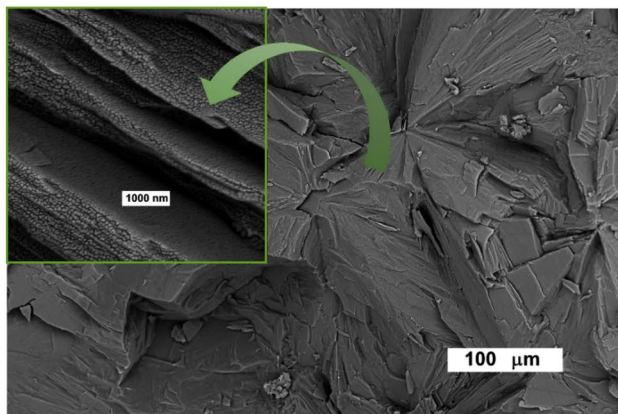
The ac conductivity (σ_{ac}) patterns of the as-prepared samples (glass ones) exhibit dispersion at higher frequencies and a frequency-independent plateau in the low-frequency range. In other words, frequency reliance of σ' is delineated on the low-frequency side by a plateau-like pattern. The characteristic frequency (ν_c), at which dispersion begins to manifest and transforms into a power law at higher frequencies, are directly derived from the plateau value as well as the dc conductivity (σ_{dc}). However, this behavior became now main feature of conducting and semiconducting materials, the interfacial polarization shown in the sintered glasses at 650 °C/2 h confirms their ability to store electrical energy [28–30]. More inspection of the figure shows



G62



G71



G0

Fig. 4 SEM micrographs of G0-, G71-, and G62-sintered glasses at 650 °C/2 h

that the heat-treated sample G0, that is, TiO₂ free sample sintered at 650 °C/2 h behaves as highly conducting glass-ceramic material. This confirms the magic influence of LiO₂ in increasing conductivity

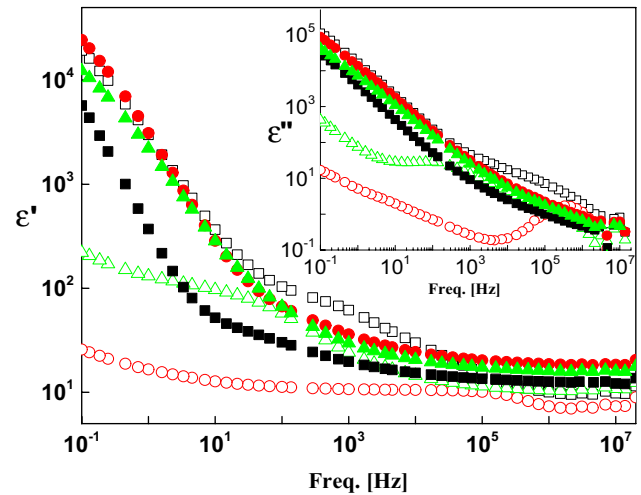


Fig. 5 Frequency dependence of permittivity, ϵ' for the three investigated glass samples, G0: black, G71: red, and G62: green. As-prepared glasses (close symbols) and sintered at 650 (open symbols). The inset shows the dielectric loss with the similar notations (Color figure online)

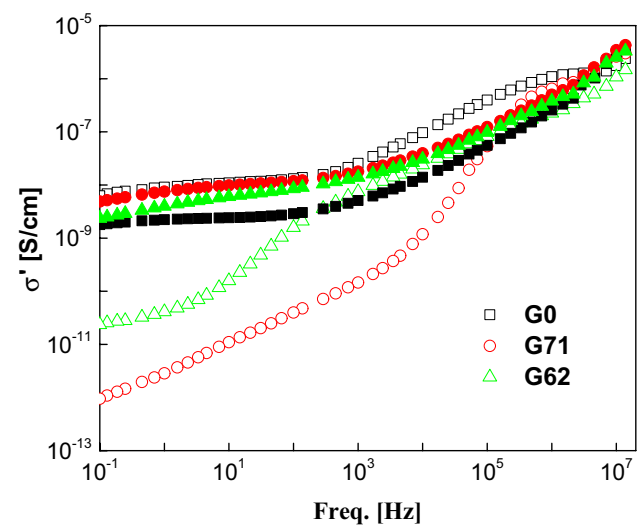


Fig. 6 The ac conductivity, σ' , for the three investigated glass samples, G0, G71 and G62. The same notations as in Fig. 5.

as compared with TiO₂. This may attributed to the less volume of the Ti.

Figure 6 depicts the calculated electric loss modulus (M'') against frequency for the three investigated glass-ceramics as compared with their as-prepared glasses G0, G71, and G62.

The electric loss modulus has been used recently in order to study the relaxation mechanism of the conductivity in many conductive materials like

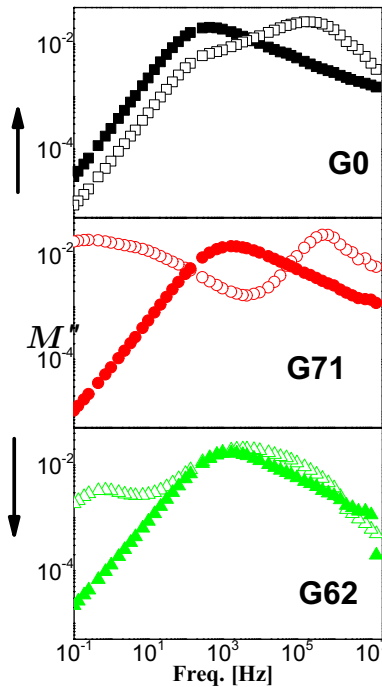


Fig. 7 Frequency dependence of electric loss modulus M'' for the three investigated glass samples as-prepared (close symbols) and sintered at 650 °C (open symbols)

conductive polymers [31, 32], conductive composites [33], ion conductive glasses [34], crystals [35], and ceramics [36]. The description of some specific relaxation processes is quite beneficial. It became well known that a conductivity contribution to the dielectric spectra shows up as a peak in the modulus representation [17, 37].

The three glass samples show only one sharp and clear peak for each sample. This peak originated from the hopping mechanism of the ions and hence the conductivity contribution. Frequency of the peak maximum position (reciprocal of the hopping time) is directly related to the dc conductivity. There is, once again, no indication of interfacial polarization meaning that all free charge carriers are involved in the transport mechanism (Fig. 7). As the three glass samples are sintered at 650 °C (open symbols in the figure), the peak of conductivity contribution shifted remarkably toward lower frequencies (the hopping mechanism became very slow and hence the glass-ceramics became insulator). However, a new clear peak related to the interfacial polarization is produced. Only the sample G0 has a comparable conductivity peak position in the two phases indicating the high conductivity even in case of G0

glass-ceramic confirming once again the effect of free ions Li^+ in enhancement of conductivity.

4 Conclusion

Through the $\text{SiO}_2\text{-Li}_2\text{O-TiO}_2$ glass system, both lithium di- and meta-silicates were developed. Combination and increase of TiO_2 relatively decreased the crystallization temperature. Although lithium disilicate crystallized at 650 °C in TiO_2 -free glass, whereas incorporation of TiO_2 simulate the crystallization of lithium metasilicate phases. Spherulitic growths were developed in the microstructure at 650 °C/2 h which nearly sorted in nanosize and spread in glassy groundmass. When the bulk glass was amorphous, it had a clear conductivity devoid of lithium mobility; but, when the glass-ceramic samples were sintered or crystalline, they behaved like insulators. Furthermore, in the case of glass-ceramic structures, there is a definite interfacial polarization that results from the accumulation of charge carriers at the interface between glassy and crystalline phases. The very high conductivity of the TiO_2 free sample confirms the impact of Li^+ free ions on the samples' electric characteristics.

Acknowledgements

The authors gratefully acknowledge the National Research Center for supporting this study with the aid of its facilities.

Author contributions

EMAH contributed to conceptualization, methodology, validation, formal analysis, investigation, resources, data curation, writing of the original draft, reviewing and editing of the manuscript, and visualization. GTEL-B contributed to methodology, validation, formal analysis, data curation, writing of the original draft, reviewing and editing of the manuscript, and visualization. MAA contributed to methodology, formal analysis, and visualization. GMT contributed to methodology, validation, formal analysis, writing of the original draft, reviewing and editing of the manuscript, and visualization.

Funding

Open access funding provided by The Science, Technology & Innovation Funding Authority (STDF) in cooperation with The Egyptian Knowledge Bank (EKB). This work did not take any specific grant from different funding agencies.

Data availability

Data will be made available on request.

Declarations

Conflict of interest The authors declare that they have no known competing financial interests or personal relationships that could have appeared to influence the work reported in this paper.

Open Access This article is licensed under a Creative Commons Attribution 4.0 International License, which permits use, sharing, adaptation, distribution and reproduction in any medium or format, as long as you give appropriate credit to the original author(s) and the source, provide a link to the Creative Commons licence, and indicate if changes were made. The images or other third party material in this article are included in the article's Creative Commons licence, unless indicated otherwise in a credit line to the material. If material is not included in the article's Creative Commons licence and your intended use is not permitted by statutory regulation or exceeds the permitted use, you will need to obtain permission directly from the copyright holder. To view a copy of this licence, visit <http://creativecommons.org/licenses/by/4.0/>.

References

- M.A. Taha, R.A. Younes, G.T. El-Bassyouni, M.A. Azooz, FTIR spectral characterization, mechanical and electrical properties of P_2O_5 - Li_2O - CuO glass-ceramics. *Silicon* **13**(9), 3075–3084 (2020). <https://doi.org/10.1007/s12633-020-00661-5>
- F.H. El-Batal, G.T. El-Bassyouni, Bioactivity of Hench bioglass and corresponding glass-ceramic and the effect of transition metal oxides. *Silicon* **3**(4), 185–197 (2011). <https://doi.org/10.1007/s12633-011-9095-6>
- M. Jakovac, M. Žic, L. Pavić, T. Klaser, Electrical properties of two types of lithium-based glass ceramics. *Acta Stomatol. Croat* **56**(3), 281–287 (2022). <https://doi.org/10.15644/asc56/3/6>
- H.A. El Batal, M.A. Azooz, G.T. El-Bassyouni, F.H. El Batal, E.M.A. Hamzawy, Crystallization of the glasses within the SiO_2 - Li_2O - TiO_2 system. *Mater. Chem. Phys.* **275**, 125216 (2022). <https://doi.org/10.1016/j.matchemphys.2021.125216>
- B. Konar, I.-H. Jung, A coupled phase diagram experimental study and thermodynamic optimization of the Li_2O - CaO - Al_2O_3 and Li_2O - CaO - SiO_2 systems, and prediction of the phase diagrams of the Li_2O - CaO - Al_2O_3 - SiO_2 system. *J. Eur. Ceram.* **40**, 2185–2199 (2020). <https://doi.org/10.1016/j.jeurceramsoc.2019.12.043>
- F. Zarone, M.I. Di Mauro, P. Ausiello, G. Ruggiero, R. Sorrentino, Current status on lithium disilicate and zirconia: a narrative review. *BMC Oral Health.* **19**, 134 (2019). <https://doi.org/10.1186/s12903-019-0838-x>
- E.M.A. Hamzawy, H.A. El Batal, M.A. Azooz, G.T. El-Bassyouni, El Batal, glasses and glass-ceramics from Li_2O - KF - TiO_2 - SiO_2 system doped with SiC . *Silicon* **15**(15), 1–9 (2023). <https://doi.org/10.1007/s12633-023-02531-2>
- E. Kleebusch, C. Patzig, T. Höche, C. Rüssel, The evidence of phase separation droplets in the crystallization process of a Li_2O - Al_2O_3 - SiO_2 glass with TiO_2 as nucleating agent—an X-ray diffraction and (S)TEM-study supported by EDX-analysis. *Ceram. Int.* **44**, 2919–2926 (2018). <https://doi.org/10.1016/j.ceramint.2017.11.040>
- A. Zandonà, E. Chesneau, G. Hensch, A. Canizarès, J. Deubener, V. Montouillout, F. Fayon, M. Allix, Glass-forming ability and structural features of melt-quenched and gel-derived SiO_2 - TiO_2 glasses. *J. Non Cryst. Solids* **598**, 121967 (2022). <https://doi.org/10.1016/j.jnoncrysol.2022.121967>
- E. Kleebusch, C. Patzig, M. Krause, Y. Hu, T. Höche, C. Rüssel, The effect of TiO_2 on nucleation and crystallization of a Li_2O - Al_2O_3 - SiO_2 glass investigated by XANES and STEM. *Sci. Rep.* **8**(1), 2929 (2018). <https://doi.org/10.1038/s41598-018-21227-x>
- D.S. Gavrilovski, N.S. Blagojević, M.P. Gavrilovski, S.R. Grujić, Glass-ceramic enamels derived from the Li_2O - Na_2O - Al_2O_3 - TiO_2 - SiO_2 system. *J. Serb Chem. Soc.* **67**(2), 127–134 (2002)
- S. Karlsson, L.G. Bäck, P. Kidkhunthod, K. Lundstedt, L. Wondraczek, Effect of TiO_2 on optical properties of glasses in the soda-lime-silicate system. *Opt. Mater. Express.* **6**(4), 1198–1216 (2016). <https://doi.org/10.1364/OME.6.001198>

13. N. Monmaturapoj, P. Lawita, W. Thepsuwan, Characterisation and properties of lithium disilicate glass ceramics in the $\text{SiO}_2\text{-Li}_2\text{O-K}_2\text{O-Al}_2\text{O}_3$ system for dental applications. *Adv. Mater. Sci. Eng.* (2013). <https://doi.org/10.1155/2013/763838>
14. R. Rashid, I. Shafiq, M.R.H.S. Gilani, M. Maaz, P. Akhter, M. Hussain, K.-E. Jeong, E.E. Kwon, S. Bae, Y.-K. Park, Advancements in TiO_2 -based photocatalysis for environmental remediation: strategies for enhancing visible-light-driven activity. *Chemosphere* (2023). <https://doi.org/10.1016/j.chemosphere.2023.140703>
15. J. Ramírez-González, D.C. Sinclair, A.R. West, Impedance and dielectric spectroscopy of functional materials: a critical evaluation of the two techniques. *J. Electrochem. Soc.* **170**, 116504 (2023). <https://doi.org/10.1149/1945-7111/ad09fa>
16. Yuriy Poplavko, (2021) The basics of dielectric spectroscopy, In: *Dielectric Spectroscopy of Electronic Materials* pp. 1–40
17. A. Karabulut, I. Orak, A. Türüt, The photovoltaic impact of atomic layer deposited TiO_2 interfacial layer on Si-based photodiodes. *Solid State Electron.* **144**, 39–48 (2018). <https://doi.org/10.1016/j.sse.2018.02.016>
18. S. Ibrahim, H.A. Abo-Mosallam, E.A. Mahdy, G.M. Turkey, Impact of high NiO content on the structure, optical, and dielectric properties of calcium lithium silicate glasses. *J. Mater. Sci. Mater. Electron. (JMSE)*. **33**, 10596–10610 (2022). <https://doi.org/10.1007/s10854-022-08045-8>
19. M.A. Moussa, A.M. Ghoneim, M.H. Abdel Rehim, S.A. Khairy, M.A. Soliman, G.M. Turkey, Relaxation dynamic and electrical mobility for poly(methyl methacrylate)-polyaniline blends. *J. Appl. Polym. Sci.* **134**, 45415–45425 (2017). <https://doi.org/10.1002/app.45415>
20. W. Wersing, Microwave ceramics for resonators and filters. *Cur Opin. Solid State Mater. Sci.* **1**, 715–731 (1996)
21. G. Sharma, M. Kaur, S. Punj, K. Singh, Biomass as a sustainable resource for value-added modern materials: a review. *Biofuels Bioprod. Bioref.* **14**, 673–695 (2020).
22. M.M. Morsi, F.H. Margha, R.M.M. Morsi, Effect of sintering temperature on the developed crystalline phases, optical and electrical properties of $5\text{ZnO-2TiO}_2\text{-3P}_2\text{O}_5$ glass. *J. Alloys Compd.* **769**, 758–765 (2018). <https://doi.org/10.1016/j.jallcom.2018.08.045>
23. S.S. Danewalia, G. Sharma, S. Thakur, K. Singh, Agricultural wastes as a resource of raw materials for developing low-dielectric glass-ceramics. *Sci. Rep.* **6**, 24617 (2016). [10.1038/srep24617](https://doi.org/10.1038/srep24617)
24. G.G. Rao, B.L. Rekha, C.A. Kumar, K. Jayant, K. Samatha, D.M. Prasad, Studies on structural and dielectric properties of $\text{Li}_{0.5}\text{Fe}_{2.5}\text{O}_4$ doped in $\text{BaTi}_{0.9}\text{Zr}_{0.1}\text{O}_3$ at higher frequency region. *Appl. Phys. A Mater. Sci. Process.* **123**, 624 (2017). <https://doi.org/10.1007/s00339-017-1220-y>
25. G. Sharma, K. Singh, Dielectric properties of the calcium silicate glass-ceramics prepared from agro-food Wastes. *Silicon* **14**(4), 1489–1496 (2022). <https://doi.org/10.1007/s12633-021-00940-9>
26. J. Li, J. Huang, H. Feng, X. Wang, X. Yin, Y. Zhang, Effect of $\text{TiO}_2/\text{SiO}_2$ molar ratio on the structure, dielectric and crystallization properties of $\text{SiO}_2\text{-TiO}_2\text{-ZrO}_2\text{-RO-Al}_2\text{O}_3$ glasses. *J. Non Cryst. Solids.* **576**, 121243 (2022). <https://doi.org/10.1016/j.jnoncrsol.2021.121243>
27. M. Chavoutier, D. Caurant, O. Majérus, R. Boulesteix, P. Loiseau, C. Jousseau, E. Brunet, E. Lecomte, Effect of TiO_2 content on the crystallization and the color of (ZrO_2 , TiO_2)-doped $\text{Li}_2\text{O-Al}_2\text{O}_3\text{-SiO}_2$ glasses. *J. Non Cryst. Solids.* **384**, 15–24 (2014). <https://doi.org/10.1016/j.jnoncrsol.2013.03.034>
28. G.M. Turkey, A.M. Fayad, G.T. El-Bassyouni, M. Abdel-Baki, Dielectric and electrical properties of MoO_3 -doped borophosphate glass dielectric spectroscopy investigations. *J. Mater. Sci. Mater. Electron. (JMSE)*. **32**, 22417–22428 (2021). <https://doi.org/10.1007/s10854-021-06728-2>
29. M. Mahdy, I. El-Zawawy, G.M. Turkey, Lead telluride nanocrystalline thin films: a broadband dielectric spectroscopy study. *Curr. Appl. Phys.* **19**, 787–793 (2019). <https://doi.org/10.1016/j.cap.2019.04.011>
30. F.H. Margha, G.T. El-Bassyouni, G.M. Turkey, Enhancing the electrical conductivity of vanadate glass system (Fe_2O_3 , B_2O_3 , V_2O_5) via doping with sodium or strontium cations. *Ceram. Int.* **45**, 11838–11843 (2019). <https://doi.org/10.1016/j.ceramint.2019.03.064>
31. M.T. Ahmed, H. Elhendawy, Z.M. Elqahtani, W.B. Elsharkawy, M.A. Azzam, T. Fahmy, Electric modulus and scaling behaviour of chitosan/PVA biopolymer blend. *Egypt. J. Chem.* **65**(1), 459–471 (2022). <https://doi.org/10.21608/EJCHEM.2021.81068.4015>
32. Z. Wang, W. Zhou, L. Dong, X. Sui, J. Zuo, H. Cai, X. Liu, Q. Chen, J. Cai, Dielectric relaxation dynamics of Al/epoxy micro-composites. *J. Alloys Compd.* **689**, 342–349 (2016). <https://doi.org/10.1016/j.jallcom.2016.07.332>
33. M.A. Moussa, M.H. Abdel Rehim, S.A. Khairy, M.A. Soliman, A.M. Ghoneim, G.M. Turkey, Electrical investigations of polyaniline/sulfonated polystyrene composites using broadband dielectric spectroscopy. *Synth. Met.* **209**, 34–40 (2015). <https://doi.org/10.1016/j.synthmet.2015.06.024>
34. P. Goel, G.V. Honnavar, K.P. Ramesh, Electrical conductivity and relaxation in lithium-doped barium vanadate glasses investigated by impedance spectroscopy. *J. Phys. Chem. Solids.* **173**, 111105 (2023). <https://doi.org/10.1016/j.jpccs.2022.111105>

35. J. Wang, C. Wang, Q. Li, Y. Yu, J. Zhang, J. Zheng, C. Cheng, Y. Li, H. Wang, High-temperature dielectric relaxations in LiF single crystals. *J. Am. Ceram. Soc.* **98**(9), 2784–2788 (2015). <https://doi.org/10.1111/jace.13663>
36. R. Kumari, N. Ahlawat, A. Agarwal, S. Sanghi, M. Sindhu, Structural transformation and investigation of dielectric properties of ca substituted $(\text{Na}_{0.5}\text{Bi}_{0.5})_{0.95-x}\text{Ba}_{0.05}\text{Ca}_x\text{TiO}_3$ ceramics. *J. Alloys Compd.* **695**, 3282–3289 (2017). <https://doi.org/10.1016/j.jallcom.2016.11.200>
37. H. Matsuura, R. Shirakashi, Exclusion of DC conductivity effect from dielectric loss spectrum using Kramers Kronig

relations for evaluation of slow dynamics of water molecules. *Jpn J. Appl. Phys.* **61**, 068003 (2022). <https://doi.org/10.35848/1347-4065/ac6afe>

Publisher's Note Springer nature remains neutral with regard to jurisdictional claims in published maps and institutional affiliations.